Survival of Heterogeneous Stress Distributions Created by Precursory Slip at Frictional Interfaces

Mathilde Radiguet,[1] David S. Kammer,[1] Philippe Gillet,[2] and Jean-François Molinari[1,*]

[1]*Computational Solid Mechanics Laboratory (LSMS), Ecole Polytechnique Fédérale de Lausanne (EPFL), IIC-ENAC, Station 18, 1015 Lausanne, Switzerland*

[2]*Earth and Planetary Science Laboratory (EPSL), Ecole Polytechnique Fédérale de Lausanne (EPFL), ICMP, Station 3, 1015 Lausanne, Switzerland*

(Received 4 July 2013; revised manuscript received 2 September 2013; published 18 October 2013)

We study the dynamics of successive slip events at a frictional interface with finite-element simulations. Because of the viscous properties of the material, the stress concentrations created by the arrest of precursory slip are not erased by the propagation of the following rupture but reappear with the relaxation of the material. We show that the amplitude of the stress concentrations follows an exponential decay, which is controlled by the bulk material properties. These results highlight the importance of viscosity in the heterogeneous stress state of a frictional interface and reveal the "memory effect" that affects successive ruptures.

DOI: 10.1103/PhysRevLett.111.164302 PACS numbers: 46.55.+d, 02.70.Dh, 46.50.+a, 62.20.Qp

Understanding how the stress state at a frictional interface evolves and leads to global sliding is critical in several fields from engineering to earthquake science. Sliding along a frictional interface is often characterized by stick-slip behavior, modeled by local static μ_s and kinetic μ_k friction coefficients. When successive slip events take place, each rupture will be affected by the state of stress of the interface left by the preceding event.

Laboratory friction experiments allow us to study the dynamics of friction at an interface [1–5]. It has been shown that when the shear load is applied on the side of the system, precursors to global sliding occur [1,6]. Slip precursors correspond to slip events that initiate at the trailing edge of the sample, at shear stresses below the macroscopic friction coefficient, and stop before propagating through the entire interface. These precursor events create stress singularities at the tip of the arrested rupture [7]. This mechanism is analog to earthquakes ruptures [8], for which stress concentrations exist at the edges of the ruptured area. Both in laboratory earthquakes and on natural faults the arrest of slip fronts dynamically generates heterogeneous stress distributions along the sliding interface, which have been shown to significantly affect rupture propagation and arrest [3,9–11].

Previous analysis of these precursor events studied how the loading conditions influence the precursor lengths [6,12,13] or the macroscopic static friction coefficient [14]. Up to now, no numerical study has analyzed the evolution of interface stresses with successive ruptures using constitutive laws describing viscoelastic material properties. Yet, to understand this evolution, numerical simulations are necessary to overcome the limitations of experimental recordings.

The simulated system, schematically shown in Fig. 1(a), consists of a two-dimensional rectangular viscoelastic solid (dimensions $w = 200$ mm and $h = 100$ mm) in contact with a rigid plane, in plane-stress approximation. The deformable solid is discretized in quadrilateral elements, and the corners of the plate are rounded to avoid stress singularities at the edges. Friction at the interface is controlled by a linear slip weakening friction law. The value of the friction coefficient linearly evolves from a value of $\mu_s = 0.7$ to $\mu_k = 0.45$ over a slip weakening distance $d_c = 1 \times 10^{-6}$ m and remains constant beyond this point. Instantaneous restrengthening to the value μ_s occurs upon the termination of slip. Regularization in the frictional strength τ^s response to normal stress σ variations is added using a simplified form of the Prakash-Clifton law [15]. The frictional strength τ^s evolution is described by $\dot{\tau}^s = -1/t^*(\tau^s - \mu\sigma)$, similar to the one proposed in Refs. [16,17]. The characteristic time scale of the regularization t^* is small compared to the duration of slip events t_s ($t^* = 5 \times 10^{-5}$ s $<< t_s \approx 1 \times 10^{-3}$ s). This regularization was shown to address the ill-posedness of ruptures on bimaterial interfaces [18] and to reduce high-frequency oscillations [19]. We use the finite-element code AKANTU [20], with an explicit Newmark-β integration scheme and the traction-at-split-node technique [21] at the interface.

We apply a constant pressure F_N (6250 N) to a rigid plate in contact with the top surface. After reaching equilibrium, a tangential loading force $F_T = K(x_1 - x_0)$ is applied to the trailing edge ($x = 0$ at the onset of calculation) via a spring of stiffness K (6×10^6 N/m) through a rigid pusher of width $w_p = 0.01$ m, located at a distance $h_p = 0.01$ m from the interface. $x_1 = V_x t$ is the position of the left end of the spring, V_x (2.5×10^{-3} m/s) corresponds to the constant driving velocity, and x_0 is the position of the pusher along the x axis.

In this study, the viscoelastic behavior of PMMA [22,23] is modeled using the standard linear solid model [24] on

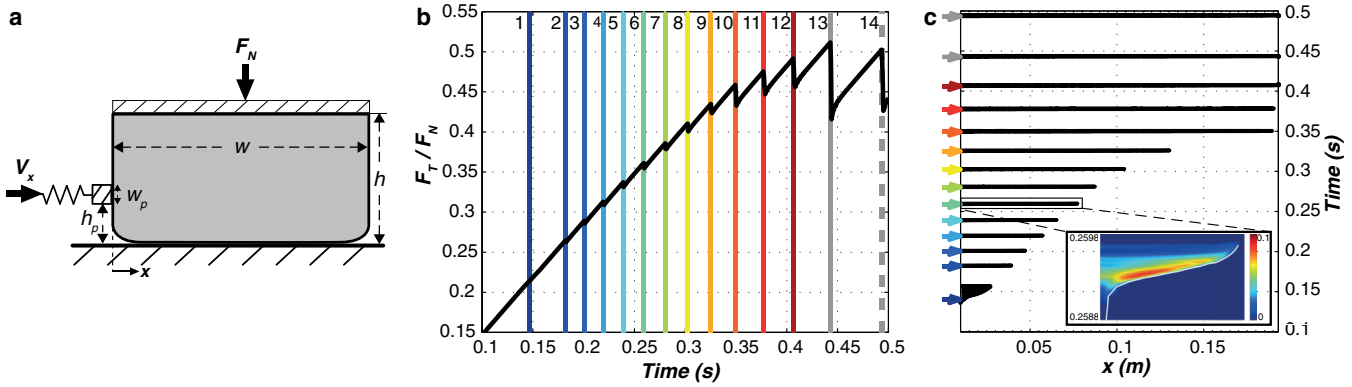

FIG. 1 (color online). (a) Two-dimensional model setup: a rectangular plate with rounded corners in contact with a rigid plane. The system is loaded on the top with a constant force F_N and from the side with a constant velocity $V_x(t)$ applied to a rigid pusher via a spring. (b) Evolution of the global forces with time. Time of slip events (precursors and global sliding) is marked with vertical bars. Precursor events are color coded from blue to red, and global sliding events are in gray. (c) Location of slipping regions along the interface over time. Slip precursors of increasing length are observed. (inset) Local slip velocities (m/s) along the interface for the 6th precursor. The white line shows the position of the rupture front.

the deviatoric part of the strain tensor (see Ref. [25] for details). The material's density ρ is 1200 kg/m^3, and the Poisson's ratio ν equals 0.37. The Young moduli are chosen using consistent experimental measurements on PMMA [22,26]. The static elastic modulus ($E_\infty = 3$ GPa) is relevant for material deformation and the dynamic modulus ($E_0 = E_v + E_\infty = 5.6$ GPa, where E_v is the viscous modulus) is relevant for the wave propagations. The effective elastic modulus E evolves from E_0 to E_∞ over the relaxation time $t_v = 1.7 \times 10^{-3}$ s. Because of the higher loading rate used in the simulation compared to that of the experiments, t_v in the simulations is significantly shorter than the one measured experimentally [23]. However, this does not affect the accuracy of our results because (i) t_v is sufficiently large so that variations in the effective E are small during events and (ii) the ratio between t_v and the interevent time is similar between simulations and experiments. We checked that we obtained similar results when varying both t_v and the interevent time (by changing V_x).

We first analyze the evolution of slip at the interface when the shear load is increased. The loading curve [Fig. 1(b), ratio of global shear force F_T over normal loading F_N] increases almost linearly with time, from an initial zero loading. Each stress drop in the curve (vertical colored line) is associated with a slip event. As observed experimentally [1,6], these slip events always initiate at the trailing edge and show increasing lengths with increasing load [Fig. 1(c)]. Precursor lengths increase linearly up to half the sample length and then increase faster to reach the leading edge ($x = 0.2$ m), causing global sliding. This behavior is due to friction-frustrated Poisson expansion. The first slip precursor has a longer duration and a slower propagation speed compared to the following events and is similar to the quasistatic precursor described in Ref. [14].

The propagation speed v_c of the slip front for the 7th to 10th precursors (Fig. 2) reveals an accelerating phase, from 0 to 0.04 m, followed by a slow decrease of v_c. During this second phase, peaks corresponding to sudden accelerations of the front can be identified. For each precursor, the last peak before rupture arrest has a large amplitude and is located at the position where the previous precursor stopped (gray bars in Fig. 2). The arrest of precursor n will lead to a strong acceleration of precursor $n + 1$ and will also create smaller accelerations of precursors $n + 2$, $n + 3$. It has been shown [3,27] that v_c is generally linked to the ratio of local shear to normal stresses τ/σ along the interface. These accelerations are thus due to stress concentrations created by the arrest of previous slip precursors. Therefore, persisting peaks of v_c over several cycles of slip events indicate that the propagation of a single rupture front does not erase all stress concentrations at the interface.

Lines from blue to gray in Fig. 3(a) show τ/σ at the interface just prior to each slip event (shifted along the y axis for clarity). The arrest location of precursor i

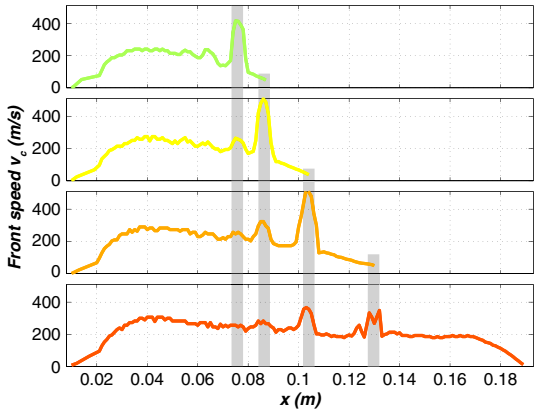

FIG. 2 (color online). Propagation speed of the front (averaged over 5 mm) for precursors 7 (top) to 10 (bottom). Gray bars highlight acceleration of the front related to the location of arrested precursors.

(position x_i, thin vertical lines) is marked by a peak of decreasing amplitude in the stress profile of the following precursors. We define the amplitude of a stress concentration $\Delta_i(\tau_n/\sigma_n)$ as the peak in τ/σ created by the arrest of the ith precursor. $\Delta_i(\tau_n/\sigma_n)$ is measured before each slip event n and is defined for $n > i$ as

$$\Delta_i\left(\frac{\tau_n}{\sigma_n}\right) = \frac{\tau_n(x_i)}{\sigma_n(x_i)} - \frac{\tau_n(x_i')}{\sigma_n(x_i')}. \quad (1)$$

x_i is the position of the arrest of the ith precursor, and $x_i' \in [x_{i-1}, x_i]$ is the position of the local minimum in $\tau(x)/\sigma(x)$. x_i' is defined for the first event $n = i + 1$ and is kept constant for the following events. A zoom around the arrest location of the 8th position [inset of Fig. 3(a)] shows how $\Delta_i(\tau_n/\sigma_n)$ is evaluated. In the following, we consider A_i^n, the difference between the amplitude of the stress concentration $\Delta_i(\tau_n/\sigma_n)$ and Δ_i^{ref}, which is the remaining stress when all stress concentrations are erased, before the last slip event $\Delta_i^{\mathrm{ref}} = \Delta_i(\tau_{14}/\sigma_{14})$. A_i^n is normalized such that the first value $A_i^{i+1} = 1$,

$$A_i^n = \frac{\Delta_i(\frac{\tau_n}{\sigma_n}) - \Delta_i^{\mathrm{ref}}}{\Delta_i(\frac{\tau_{i+1}}{\sigma_{i+1}}) - \Delta_i^{\mathrm{ref}}}. \quad (2)$$

The evolution of the A_i^n with successive passing fronts presents the same exponential decrease rate, for all precursor arrest positions x_i [dots in Fig. 3(b) and inset].

We will show that these stress concentrations appear due to viscoelasticity of the bulk material. The friction law used implies that τ/σ is close to μ_k when slip terminates. Thus, just after the propagation of a slip event, all previous stress concentrations are erased, and a peak only exists at the tip of the arrested rupture [dark blue line in Fig. 3(c)]. With time, the bulk relaxes and the stress concentrations reappear before the next event [dark red line in Fig. 3(c)]. Figure 3(d) shows the time evolution of τ at a given position x_7. Three slip events can be identified in the figure (peaks and drops in τ). During the interevent time, τ increases due to the relaxation of the bulk following the drop and to the external shear loading. In the following, we model this evolution. Assuming, at equilibrium, an instantaneous stress drop $\Delta\tau_n(x)$ due to the slip event n occurring at time t_n, the relaxation in τ can be described by

$$\tau(x, t) = \tau(x, t_n + \epsilon) + p_\tau(x)(t - t_n) + \frac{E_v}{E_0}\Delta\tau_n(x)\{1 - \exp[-(t - t_n)/t_v]\}, \quad (3)$$

where $\tau(x, t_n + \epsilon)$ is the shear stress immediately after the slip event and $p_\tau(x)$ is the shear loading rate in x. Since in our calculations the slip at the interface is larger than d_c, $\tau(x, t_n + \epsilon) = \mu_k\sigma(x, t_n + \epsilon)$. Considering the normal loading rate $p_\sigma(x)$, and neglecting the viscous effect on σ, the normal stress just before event $n + 1$ is $\sigma_{n+1}(x) = \sigma(x, t_n + \epsilon) + p_\sigma(x)(t_{n+1} - t_n)$. Moreover, the shear stress drop due to event n is $\Delta\tau_n(x) = \gamma\{\tau_n(x) - \mu_k[\sigma_{n+1}(x) - p_\sigma(x)(t_{n+1} - t_n)]\}$. The factor γ $(0 < \gamma < 1)$ accounts for the time history of the drop. For an instantaneous drop $\gamma = 1$ and in real cases, because of the drop's duration, $\gamma < 1$.

If the relaxation time t_v is considerably shorter than the interevent time $t_{n+1} - t_n$, almost complete relaxation occurs and the exponential in Eq. (3) can be neglected. The shear stress just before event $n + 1$ will thus have the following expression:

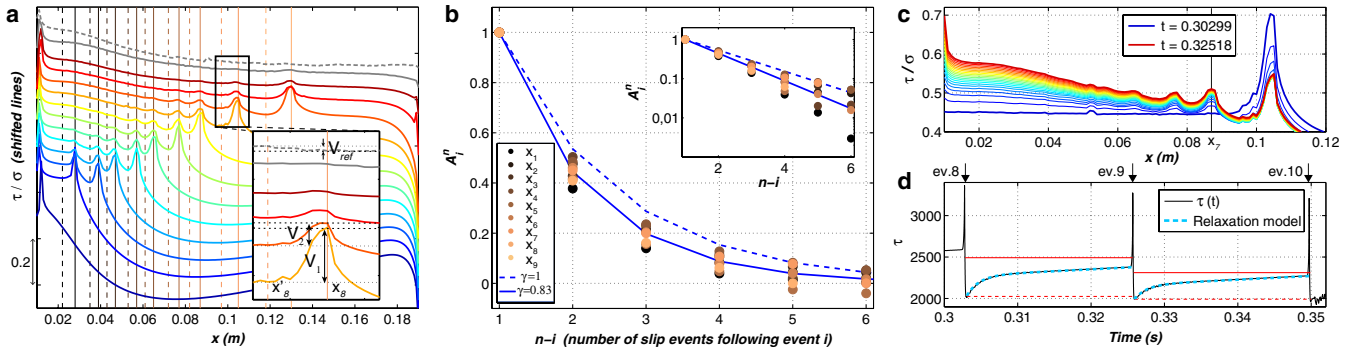

FIG. 3 (color online). (a) Local τ/σ ratio along the interface just prior to each slip event. Colors from blue to gray correspond to successive slip events (see Fig. 1 for color code). Lines are shifted along the y axis for clarity. Continuous and dashed vertical lines correspond, respectively, to the positions x_i and x_i'. (inset) Zoom around the position x_8; $\Delta_i(\tau_n/\sigma_n)$ is the variation in τ/σ between x_8 and x_8'. Simplified notations correspond to $V_1 = \Delta_8(\tau_9/\sigma_9)$, $V_2 = \Delta_8(\tau_{10}/\sigma_{10})$, and $V_{\mathrm{ref}} = \Delta_8(\tau_{14}/\sigma_{14})$ and highlight the decreasing amplitude of stress concentrations A_i^n [Eq. (2)]. (b) Normalized amplitude of stress concentration A_i^n as a function of the number of slip events after event i. Colors correspond to different positions x_i. Dotted and continuous blue lines correspond to a decrease rate of $\gamma(E_v/E_0)$ with $\gamma = 1$ and $\gamma = 0.83$, respectively. (inset) Same data points with A_i^n in log scale reveal the exponential decay of stress concentration. (c) Lines show the time evolution of τ/σ from blue (just after the 8th event) to red (just before the 9th event). The horizontal black line shows x_7, for which time evolution is shown in (d). (d) Time evolution of $\tau(x_7)$ [position of black line in (c)] during two slip event cycles. The modeled behavior [dashed cyan line, Eq. (3)] closely matches the data (thin black line). The amplitude between the two red lines is $\gamma\Delta\tau_n$ with $\gamma = 0.83$.

$$\tau_{n+1}(x) = \mu_k \sigma_{n+1}(x) + \gamma \frac{E_v}{E_0}[\tau_n(x) - \mu_k \sigma_{n+1}(x)] + \left[p_\tau(x) + \mu_k p_\sigma(x) \left(\gamma \frac{E_v}{E_0} - 1 \right) \right] (t_{n+1} - t_n). \quad (4)$$

In the following, we assume that variations in σ are negligible. We can now express A_i^n using Eq. (4). The loading-dependent terms (p_τ and p_σ) appear in both $\Delta_i(\tau_n/\sigma_n)$ and Δ_i^{ref}, and thus cancel out. If we consider an elastic medium with no viscosity ($E_v = 0$), then $A_i^n = 0$ after the propagation of a slip event at the position x_i, i.e., for $n - i > 1$. Thus, in the elastic case, stress concentrations are erased by slip and no survival of heterogeneous stress distribution exists.

For a viscoelastic material, A_i^n evolves with successive ruptures following:

$$A_i^n = \left(\gamma \frac{E_v}{E_0} \right)^{n-i-1}. \quad (5)$$

As shown in Fig. 3(b), $\gamma = 1$ overpredicts the decrease rate of stress concentrations. A best-fit curve is obtained with $\gamma = 0.83$, which integrates the duration of the drop in τ. This value gives a good prediction of the observed behavior, both in Fig. 3(b) and in the time evolution of τ in Fig. 3(d). The relation in Eq. (5) is valid when the viscoelastic material has sufficient time to relax between two events, which is the case in the present simulations where $t_{n+1} - t_n \approx 2 \times 10^{-2}$ s $\gg t_v$. When $t_{n+1} - t_n < 3t_v$, the relaxation is not fully accomplished and A_i^n decreases faster. If $t_{n+1} - t_n < 0.01 t_v$, less than 1% of the stress concentration reappears before the event $n + 1$, and heterogeneous stress distributions do not survive. A more complex model for PMMA viscoelasticity, including several time scales, could be considered. In this case, the same relation between each time scale and $t_{n+1} - t_n$ applies.

The results of the present finite-element simulation showed that the dynamics of a slip event is strongly influenced by the history of slip at the interface. Stress concentrations are created by the arrest of precursory slip events. After the propagation of a slip front, they reappear due to the viscoelastic relaxation and, thus, survive the propagation of several successive slip fronts. All stress concentrations follow a similar exponential decrease rate, controlled by $\gamma E_v/E_0 = 0.44$. Equation (5) and Fig. 3(b) show that for the parameters selected here, the stress concentration is only 1.6% of its initial value after the propagation of five slip events.

The viscous relaxation is seen by the change of slope in Fig. 1(b), where just after a slip event the loading increases faster and then slows down towards a linear rate. The same behavior seems to be observed in the experimental measurements (Fig. 1a in Ref. [1]), and we suggest this may also come from the viscoelasticity. Other evidences of this effect have not yet been observed experimentally and may be related to the difficulty in obtaining dense measurements of interfaces stresses.

The decrease rate of the stress concentrations is controlled by the ratio between E_v and E_0 and the ratio between the relaxation time t_v and the interevent time. In the present study, complete relaxation occurs between slip events. The incorporation of a rate-dependent friction law, or aging effects, would create heterogeneous frictional strength at the interface. The resulting complexity in the stress field would add to the stress concentrations studied here.

Recent laboratory friction experiments highlight the importance of viscoelastic properties in the size distribution of slip events and the importance of the loading rate (which controls the interevent time) [28]. At a larger scale, seismologic and geodetic observations reveal, among other mechanisms, the role of viscous relaxation in postseismic stress transfer and its importance for seismic hazard assessment [29–31]. The present study highlights the importance of viscous relaxation mechanisms in the survival of heterogeneous stress states along frictional interfaces. Over different time scales, similar mechanisms could exist around geological faults and help in the understanding of the importance of the previous slip history in earthquake ruptures.

The authors are grateful to F. Renard for his comments on the importance of memory effects at frictional interfaces, and to J.-P. Ampuero for a helpful discussion on the role of viscoelasticity. The research described in this article is supported by the Swiss National Science Fundation (Grant No. PMPDP2_145448) and the European Research Council (ERCstg UFO-240332).

*jean-francois.molinari@epfl.ch

[1] S. M. Rubinstein, G. Cohen, and J. Fineberg, Phys. Rev. Lett. **98**, 226103 (2007).
[2] S. M. Rubinstein, G. Cohen, and J. Fineberg, Nature (London) **430**, 1005 (2004).
[3] O. Ben-David, G. Cohen, and J. Fineberg, Science **330**, 211 (2010).
[4] S. Latour, T. Gallot, S. Catheline, C. Voisin, F. Renard, E. Larose, and M. Campillo, Europhys. Lett. **96**, 59 003 (2011).
[5] K. Xia, A. J. Rosakis, and H. Kanamori, Science **303**, 1859 (2004).
[6] S. Maegawa, A. Suzuki, and K. Nakano, Tribol. Lett. **38**, 313 (2010).
[7] Y. Bar-Sinai, R. Spatschek, E. A. Brener, and E. Bouchbinder [arXiv:1306.3658 (to be published)].
[8] O. Ben-David, G. Cohen, and J. Fineberg, Tribol. Lett. **39**, 235 (2010).
[9] B. T. Aagaard and T. H. Heaton, J. Geophys. Res. **113**, B04301 (2008).
[10] R. Madariaga and A. Cochard, Proc. Natl. Acad. Sci. U.S.A. **93**, 3819 (1996).

[11] L. Rivera and H. Kanamori, Geophys. Res. Lett. **29**, 12 (2002).
[12] J. Trømborg, J. Scheibert, D. S. Amundsen, K. Thøgersen, and A. Malthe-Sørenssen, Phys. Rev. Lett. **107**, 074301 (2011).
[13] D. Amundsen, J. Scheibert, K. Thøgersen, J. Trømborg, and A. Malthe-Sørenssen, Tribol. Lett. **45**, 357 (2012).
[14] M. Otsuki and H. Matsukawa, Sci. Rep. **3**, 1586 (2013).
[15] V. Prakash and R. Clifton, in *Experimental Techniques in the Dynamics of Deformable Solids*, edited by A. K. T. Ramesh (American Society of Mechanical Engineering, New York, 1993), Vol. 165, pp. 33–48.
[16] M. D. Bartolomeo, F. Massi, L. Baillet, A. Culla, A. Fregolent, and Y. Berthier, Tribol. Int. **52**, 117 (2012).
[17] N. DeDontney, J. R. Rice, and R. Dmowska, Bull. Seismol. Soc. Am. **102**, 541 (2012).
[18] A. Cochard and J. R. Rice, J. Geophys. Res. **105**, 25 891 (2000).
[19] D. Kammer, V. A. Yastrebov, G. Anciaux, and J. F. Molinari, J. Mech. Phys. Solids (to be published).
[20] AKANTU, http://lsms.epfl.ch/akantu.
[21] D. J. Andrews, Bull. Seismol. Soc. Am. **89**, 931 (1999).
[22] M. Ciccotti and F. Mulargia, Geophys. J. Int. **157**, 474 (2004).
[23] S. Rabinowitz and N. Brown, J. Polym. Sci. B **39**, 2420 (2001).
[24] C. Zener, *Elasticity and Anelasticity of Metals* (University of Chicago, Chicago, 1948).
[25] J. Simo and T. Hughes, *Computational Inelasticity* (Springer-Verlag, New York, Berlin, Heidelberg, 1998).
[26] J. Fineberg (private communication).
[27] D. S. Kammer, V. A. Yastrebov, P. Spijker, and J. F. Molinari, Tribol. Lett. **48**, 27 (2012).
[28] T. Yamaguchi, M. Morishita, M. Doi, T. Hori, H. Sakaguchi, and J.-P. Ampuero, J. Geophys. Res. **116**, B12306 (2011).
[29] S. Barbot and Y. Fialko, Geophys. J. Int. **182**, 1124 (2010).
[30] A. M. Freed and J. Lin, Nature (London) **411**, 180 (2001).
[31] A. M. Freed, Annu. Rev. Earth Planet. Sci. **33**, 335 (2005).